Growth and morphology in Langmuir monolayers

A. Flores[1], E. Corvera-Poiré[2], C. Garza[1] and R. Castillo[1]

[1] *Instituto de Física, UNAM - P. O. Box 20-364, D. F., 01000 Mexico*
[2] *Facultad de Química, UNAM - Cd. Universitaria, D. F., 04510 Mexico*

Abstract. – We show that domain growth of condensed phases from a metastable phase in Langmuir monolayers presents several stages. At the very beginning, depending on the supersaturation level, structures evolve through a tip-splitting dynamics. If supersaturation levels are high, there is a morphological transition, domains grow with needle tips that show as growth proceeds, side branching. The way in which the instability starts at round domains when a small lateral pressure jump is applied to the monolayer is also shown. A model for a monolayer interacting with the subphase is presented. This model can be related to the theory of dynamic phase transitions, where morphological structures and morphological transitions are predicted.

Introduction. – Insoluble amphiphilic molecules form Langmuir monolayers (LMs) at the air-water interface. LMs are studied using measurements of pressure-area isotherms, $\Pi(A,T) = \gamma_0(T) - \gamma(A,T)$, where T is the temperature, A is the area/molecule, γ and γ_0 are the surface tensions of the monolayer and of pure water, respectively, and using some observational technique like Brewster angle microscopy (BAM). In this letter, we present a study of how patterns formed by monolayer domains of a stable phase, usually a solid or liquid condensed phase, propagate into a metastable one, usually a liquid expanded phase. During this propagation, the interface between the two phases moves as the metastable phase is transformed into the stable one. The interface becomes unstable and forms patterns as a result of the competition between a chemical potential gradient that destabilizes the interface on one hand, and line tension that stabilizes the interface on the other. The further the system is out of equilibrium the faster the metastable phase will turn into the stabler phase and, consequently, the faster the interface will propagate. The competition between effects that stabilize and destabilize the system gives rise to characteristic length scales of growing domains and determines together with the anisotropy, the overall shape and symmetry of domain patterns. Balance between competing effects varies as growth conditions change. The observed patterns may be grouped into a small number of typical patterns or morphologies each representing a different dominant effect. For a given system, each morphology is observed over a range of growth conditions.

In single-component LMs the problem of non-equilibrium growth morphologies is subtler than in 3D solids. In the latter case, the role played by the released heat during the phase transition, which has to be diffused away from the interface before the front can advance further, is not important in LMs, because the monolayer rests on a large body of water (subphase) that acts as an isothermal reservoir, absorbing all the latent heat released during the phase transition. In monolayers, growing instabilities are usually observed along a fluid/non-fluid

phase transition, where the involved phases have a large difference in area density ($\sim 50\%$). Supersaturation induces domain growth, which depending on the experimental conditions, forms fractal, seaweed, and dendritic morphologies.

Pattern formation in 3D has a long history [1,2]. The selection problem for growing needle crystals was solved through the micro-solvability theory, with the conclusion that surface tension and surface kinetics, despite their small size, turned out to be singular perturbations to the problem that totally change the character of interfacial dynamics [3,4]. When surface tension and surface kinetics are isotropic, dendritic growth does not occur, but rather fingers with tip splitting dynamics. Anisotropy is required in the interfacial dynamics to produce dendritic growth [2,5–7]. A theory of pattern formation for diffusional growth has been presented, which is able to develop a morphology diagram [8–11]. Here, the building block for the dendritic structure is a dendrite with parabolic tip, and the basic element for the seaweed structure is a doublon [12,13]. The control parameters in the morphology diagram are the anisotropy, ε, of the capillary length and the undercooling, Δ; structures are classified according to whether they are compact or fractal, and whether they posses orientational order or not. Many experiments have been performed to understand the solidification problem in 3D. However, experimental studies of 2D patterns formed by monolayer domains when a stable phase is propagating into a metastable one are not common. Miller and Möhwald [14] worked with a phospholipid monolayer and explained their observations in terms of a diffusive model with impurities, since they used a dye to observe the monolayer with polarized fluorescence microscopy; they observed structures that correspond to seaweed growth. Using the same observational technique, a chiral amphiphile was studied [15]. More recently, monolayer observations are made with the non-invasive BAM. A variety of non-equilibrium growth structures has been found for monolayers [16–18], although in these studies the observed instability was not discussed. Flores *et al.* [19], observed dendritic growth for DODA monolayer caused by supersaturation and Bruinsma *et al.* [20] have proposed a hydrodynamic mechanism based on Marangoni flow to describe growth instabilities.

Results and discussion. – Here, we present how, at some point during the domain growth, there is a morphology transition from tip splitting to side branching. This was observed for three different Langmuir monolayers using BAM: dioctadecylamine (DODA), ethyl palmitate (EP), and ethyl stearate (ES). In particular, to observe the domain growth of the S_1 phase in DODA monolayer, we performed several experiments where the monolayer was compressed up to the phase coexistence of LE and S_1. After few minutes of relaxation ($\sim 15\,\mathrm{min}$), a pressure jump was made by a sudden compression of the monolayer to supersaturate the system. This sudden compression created the equivalent of undercooling in classical solidification. The pressure reached after the jump was maintained constant. Jumps of the same size were repeated several times consecutively to increase the supersaturation level at each jump. After the initial jump, domains usually were very small, and the smaller ones melted again during the observation time. At larger supersaturations (second or third pressure jump), the size of domains allowed for a clear observation of them, using BAM. Further jumps were in general useless, since domains became large and big enough to interact among them. In a first experiment, we made jumps of $\Delta\Pi = 1\,\mathrm{mN/m}$, and after the third jump, when a pressure of $\Pi = 9\,\mathrm{mN/m}$ was reached, the monolayer initially presented flower-like domains formed by 5–7 leaves, not very symmetric, and most of the times, bulged at the ends; some of them showed tip splitting. Thereafter, domains grow on average, with a seaweed-like structure caused by the typical tip-splitting dynamics (fig. 1a). However, since the local growing conditions along the trough were not exactly the same, it was usual to observe some locations along the monolayer with domains showing tip splitting and others showing thick arrow-shaped tips. Figure 1b shows
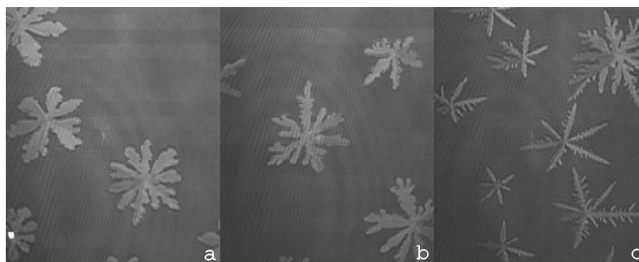
Fig. 1 – BAM images of the DODA monolayer. a) After pressure jumps of $\Delta\Pi = 1\,\text{mN/m}$ that reach a final *pressure* of $\Pi = 9\,\text{mN/m}$ ($T = 24.2\,°\text{C}$). b) After pressure jumps of $\Delta\Pi = 2\,\text{mN/m}$ that reach a final pressure of $\Pi = 8\,\text{mN/m}$ ($T = 23.6\,°\text{C}$). c) After a pressure jump of $\Delta\Pi = 4\,\text{mN/m}$, that reached a final pressure of $\Pi = 8\,\text{mN/m}$ ($T = 23.5\,°\text{C}$). The horizontal full width is $220\,\mu\text{m}$ for each image.

BAM images of the DODA monolayer ($T = 23.6\,°\text{C}$) after pressure jumps of $\Delta\Pi = 2\,\text{mN/m}$ that reached the final pressure of $\Pi = 8\,\text{mN/m}$ (second jump). At this saturation level, the monolayer seems to cross a transition zone, growing with a dynamics for which tip-splitting and side-branching morphologies were equally likely. Depending on the observed location in the monolayer, we could observe seaweed structures or dendrites, although the later ones were not well formed. It was very common to observe mixed domains, *i.e.*, domains with some legs showing tip splitting and some legs showing needle tips; in the later case, even showing side-branches (usually the larger ones). Figure 1c shows BAM images of DODA monolayer ($T = 23.5\,°\text{C}$) after a pressure jump of $\Delta\Pi = 4\,\text{mN/m}$, that reached a final pressure of $\Pi = 8\,\text{mN/m}$ (after the first jump). Here, the supersaturation was larger than in the two preceding examples. In this case, even though initially there were some domains showing tip splitting and some deformed seaweeds turning into dendrites, it was more common to observe domains with six dendritic legs with clear side branching. Finally, a global observation of figs. 1, where the essential difference is just the size of the pressure jumps that leads to different supersaturation levels (temperature is almost the same), makes it clear that, at low supersaturation levels, seaweed growth is preferred. On the contrary, at large supersaturation levels, dendritic growth is preferred.

When ES monolayer was compressed at relatively high speed ($80\,\text{cm}^2/\text{min}$, at $T = 32\,°\text{C}$), it was possible to catch the growth of domains just from the beginning, from nearly round domains up to dendritic domains. Initially, there are small round domains, the instability deforms the 1D interface and forms fingers; some of the fingers grow faster and form flower-like domains. In a next stage, the fingers turn into legs that show tip splitting. In the next events, growth is very rapid, and since the local conditions are slightly different along the monolayer, domains show mixed growing dynamics, *i.e.*, parts of a domain grow through tip splitting and other parts present needles, which quickly show side branching. At the end, before domains collide, the legs present a clear dendritic morphology (see fig. 2; a film can be seen at: `http://www.fisica.unam.mx/liquids/movies/movies.html`). EP monolayer shows exactly the same pattern. These experiments clearly show that there is a morphology transition during domain growth of a condensed phase into the metastable fluid LE phase.

Dendrite tip radius was measured on electronic images coming from BAM as function of dendrite length. We fit a circle to the tip of fully developed dendritic legs (resolution $0.5\,\mu\text{m}$) and measured the distance from that tip to the domain centre to which the dendritic legs were attached. The tip radius is almost insensitive to the dendrite length, probably revealing that the supersaturation level is similar for all dendrites in these experiments, as well as the level of line tension anisotropy; therefore, there is a selected tip radius [9]. For all measured dendrites, the tip radius was around $1.5\,\mu\text{m}$ depending on the experimental conditions. Our results here
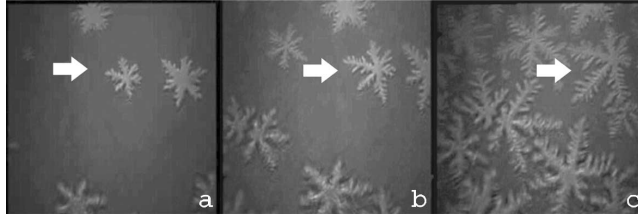
Fig. 2 – BAM images showing ethyl stearate L_2' phase growing into the LE phase at relatively high speed (time difference between images $\sim 2\,\mathrm{s}$). The monolayer was compressed at $80\,\mathrm{cm^2/min}$, at $T = 32\,^\circ\mathrm{C}$. The horizontal full width is $430\,\mu\mathrm{m}$/image. Arrows indicate a particular growing domain.

are just an estimate, since we are close to the resolution limit of the BAM technique. The position of the side branches was measured from the domain centre. Although, the side-branches at the right and at left sides are at different positions, both are disposed in a periodic way. The relation is almost linear; the linear correlation fitting coefficient is greater than 0.9 for each dendritic leg. The average distance between side branches is $5.9 \pm 1.2\,\mu\mathrm{m}$, and the average ratio of this periodicity and the measured tip radius for each dendrite leg is 3.8 ± 0.5. This number is similar to the quasi-2D dendrites obtained in NH_4Br [21]. Figures 3a and b present examples of doublons formed after a small pressure jump in LMs. Although they are astonishing, as growth proceeds the channel that characterizes them becomes, in general, wider. Figure 3c shows an AFM image of a Langmuir-Blodgett monolayer transferred on mica, where we can observe the channel of the doublon. The height difference between the domain plateau and the LE phase level is ca. $0.85\,\mathrm{nm}$ due to the different tail tilting between the S_1 and the LE phases in this monolayer.

To study the instability of the circular shape, we used monolayers made of ES and of EP whose relaxation times are short. In these experiments, the monolayers were compressed gently up to the LE/L_2' phase transition, where round domains could be clearly observed with BAM; they were allowed to relax for $\sim 5\,\mathrm{min}$. We then made a sudden compression of the monolayer that produced a lateral pressure jump. If the pressure jump is small ($\sim 1\,\mathrm{mN/m}$), the 1D circular interface deforms with a long wavelength ondulation. If pressure jumps are a little bit larger ($\sim 2\,\mathrm{mN/m}$), an instability starts to develop. Structures similar to small fingers appear and grow at the interface line. As an example, in fig. 4 we present images of growing fingers from round domains of EP at LE/L_2' phase transition after a lateral pressure jump. Since we are able to observe the early stages of the destabilization, we report frequency histograms of distances, λ, between fingers. This distance was actually measured as the
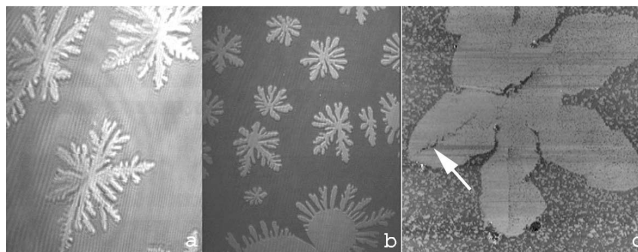

Fig. 3 – Doublons formed in Langmuir monolayers. a) DODA $T = 23.8\,^\circ\mathrm{C}$, $\Pi = 5\,\mathrm{mN/m}$. b) Ethyl palmitate $T = 20.3\,^\circ\mathrm{C}$, $\Pi = 6\,\mathrm{mN/m}$. Horizontal full width is $220\,\mu\mathrm{m}$. c) AFM images (phase lag) of a LB transferred DODA monolayer on mica. The horizontal full width is $13.5\,\mu\mathrm{m}$; temperature and pressure of LB transferring: $T = 25.6\,^\circ\mathrm{C}$ and $\Pi = 6\,\mathrm{mN/m}$. The doublon channel is shown by an arrow.
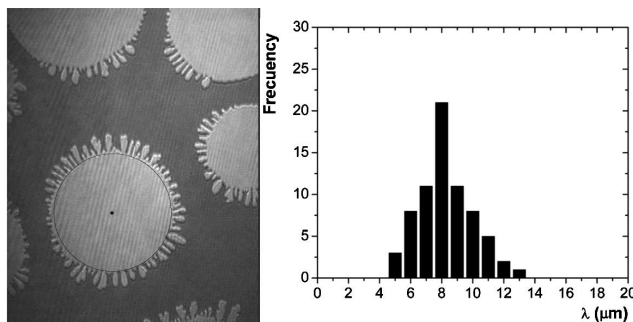
Fig. 4 – Growing fingers from round domains of ethyl palmitate at LE/L$'_2$ phase transition after a small lateral pressure jump, and a frequency chart *vs.* λ for the domain marked with a circle and a centre, showing how many fingers are found at λ (domain radius 100.4 μm).

distance between neighbouhoring valleys that have a finger between them (valley-to-valley distance). The histograms show a maximum at the most frequent value of λ. This implies that there is a wavelength that grows faster than the others, indicating that the competition between stabilizing and destabilizing effects leads to a dynamics in which some modes grow, some modes decay, and there is a mode that grows faster than the others and determines the characteristic length of the pattern at short times. This is consistent with typical dispersion relations of classical free-boundary problems.

As mentioned, in monolayers, the involved phases have a large density difference, of the order of 50%. As a result, domain growth will necessarily give rise to a density profile in the domain neighborhood. Therefore, mass diffusion must be a key variable to understand domain growth in LMs. Let us consider a LM with two coexisting phases in thermodynamic equilibrium. Here, we will represent by LE the liquid expanded phase, and by LC any condensed phase, with a long-range or with a quasi–long-range order in an order parameter. We denote by μ the chemical potential of amphiphile molecules. This one is the same for both phases when the interface is flat or when the interface curvature is negligible; let us denote it by $\mu_{\rm o}$. $\rho_{\rm l}$ and $\rho_{\rm s}$ are the amphiphile densities for LE and LC phases, respectively. If we impose a small, but abrupt, decrease in the total area occupied by the LM, as in the experiments described above, a transient increase in surface pressure ensues. Far from the LE/LC line boundary, both the amphiphile density and chemical potential in the LE phase increase by amounts $\delta\rho$ and $\delta\mu$, respectively. The chemical potential μ_0 and the density ρ_s in the LC phase change only by a negligible amount. For sufficiently low levels of supersaturation, *i.e.*, for sufficiently small values of $\delta\rho$ and $\delta\mu$, the condition of local thermodynamic equilibrium can be used. Under these conditions, we reach a stationary state, where the chemical potential is a continuous function of position, and it must be equal on both sides of the LE/LC flat line boundary. Away from this LE/LC line boundary, μ increases monotonically until it reaches a value $\mu_\infty = \mu_0 + \delta\mu$ at the monolayer boundary. The chemical potential gradient in the LE phase is the thermodynamic force that drives amphiphile molecules towards the LE/LC line boundary. Concomitant with the chemical potential, density increases monotonically from the line boundary until it reaches the asymptotic value $\rho_\infty = \rho_0 + \delta\rho$. For monolayer domains of a specific radius, local thermodynamic equilibrium at the interface implies that we must consider the Gibbs-Thomson equation:

$$\mu(\text{interface}) - \mu_0(T) = -\frac{\tau}{\Delta\rho}\kappa, \tag{1}$$

where κ is the local curvature, $\Delta\rho$ is the equilibrium density difference between LE and LC phases at the temperature T, and τ is the line tension. The subphase is treated as an

incompressible fluid where the subphase velocity field $\boldsymbol{v}(v_x, , v_y, , v_z)$ and the pressure field $P(x, y, z)$ can be calculated at the stationary state, using the Stokes' hydrodynamic equation $\eta \nabla^2 \boldsymbol{v} = \nabla P$ with $\nabla \cdot \boldsymbol{v} = 0$; here, η is the subphase viscosity. Let us denote by $\boldsymbol{u}(r, \theta)$ the monolayer velocity that follows a 2D Stokes equation, which can be written according to Bruinsma *et al.* [20] in the following way:

$$\eta_s \nabla^2_\perp \boldsymbol{u} = \nabla \Pi - \eta \partial_z \boldsymbol{u}, \tag{2}$$

where, η_s is the interfacial shear viscosity for the LE phase and $(-\eta \partial_z \boldsymbol{u})$ is the viscous stress exerted by the subphase. In order to compare surface and bulk viscous terms in eq. (2), modes of wave vector $\boldsymbol{q}$ have been considered [20]. The ratio of the interfacial to subphase viscous terms ($\zeta = \eta_s / \eta$) is of the order $q\zeta$, therefore, there are two regimes: Surface viscous losses are dominant when $q\zeta \gg 1$ and subphase viscous terms dominate when $q\zeta \ll 1$. Bruinsma *et al.* [20] estimated that for monolayers the surface-viscous regime applies. Here, the flow profile is determined by the solutions of a purely 2D Stokes equation:

$$\eta_s \nabla^2_\perp \boldsymbol{u} \approx \nabla \Pi. \tag{3}$$

On applying $\nabla_\perp \cdot$ to both sides of eq. (3), and considering in a first approximation the monolayer as incompressible (both LE and LC phases), it gives

$$\nabla^2_\perp \Pi = 0. \tag{4}$$

To first order in the gradients, eq. (4) gives $\nabla^2_\perp \rho = 0$, and finally

$$\nabla^2_\perp \mu = 0. \tag{5}$$

Therefore, we have obtained that the monolayer growth is governed by Laplace's equation, in the steady state. Equation (5) has to be solved with two boundary conditions at the interface given by the Gibbs-Thomson boundary condition, eq. (1), and the conservation boundary condition:

$$v_n = \frac{M}{\Delta \rho}[\beta(\nabla_\perp \mu)_s - (\nabla_\perp \mu)_l] \cdot \boldsymbol{n}, \tag{6}$$

where, v_n is the normal velocity to the interface, and $\beta = M'/M$ is the ratio of LC to LE mobilities, M' and M, respectively; the diffusion coefficient is $D = M(\partial \mu / \partial \rho)$.

It is important to note that eq. (5), with the boundary conditions at the interface (eqs. (1) and (6)), is similar to the equations used by Müller-Krumbhaar and collaborators [8–11] to analytically build the kinetic phase diagram, if we would include in the Gibbs-Thomson equation a supersaturation parameter Δ, and a capillary length with an anisotropy parameter ε, *i.e.*, $d = d_o (1 - \varepsilon \cos n\theta)$ [8–11]. Here, d_o is the so-called capillary length defined by $d_o = \tau \left[(\Delta \rho)^2 (\frac{\partial \mu}{\partial \rho}) \right]^{-1}$ [2]. The diagram predicted by those authors has regions of different morphological structures and lines indicating transitions between such morphological structures, where the control parameters are the degree of undercooling and the strength of anisotropy in the solid phase. They could discriminate between compact structures and fractal structures, as well as between structures with orientational order, like dendritic structures, and structures without apparent orientational order, as seaweed structures. Therefore, this is the underlying reason to have dendritic and seaweed structures in monolayers: the equation governing the monolayer is Laplace equation in the chemical potential. The transitions between morphological structures must be related to moving the control parameters, supersaturation level and line tension anisotropy, through the boundary lines along the morphological phase diagram.

Finally, using our model, we performed a linear stability analysis for a slightly perturbed round domain, whose radius is given, $R = R_o + \delta_n \cos n\theta e^{\omega t}$, where δ_n is a small deformation

amplitude. Thus, using eqs. (5), (1) and (6), and calling to Δ to the supersaturation far away from the circle, that is, $U(R_\infty) = -\Delta$, we obtain the following dispersion relation for our problem:

$$\omega_n = [n-1]\frac{v_R}{R_o}\left[1 - \frac{n(n+1)Dd_o[\beta+1]}{v_R R_o^2}\right],\tag{7}$$

where ω_n denotes the growth rate of the perturbation. The right-hand side of this formula contains two parts: a positive destabilizing term, which is proportional to the velocity and a negative stabilizing term, which contains the surface tension. This result is in agreement with classical dispersion relations and could explain why, in the experiments presented above, addressed to study the manner in which the circular shape becomes unstable there is a dominant wavelength.

Conclusion. –   We have showed that in monolayers, the domain growth of condensed phases from a metastable phase presents several stages. Some unstable modes grow faster than others and structures evolve through a tip-splitting dynamics. At high supersaturation levels, there is a morphological transition. Domains start to grow with needle tips, which show as growth proceeds, side branching. In addition, we showed how the instability starts at round domains when a small lateral pressure jump is applied to the monolayer and it is consistent with classical linear stability results for free-boundary problems. Finally, we have presented a model for a monolayer interacting with the subphase which can be related to the theory of dynamic phase transitions developed by Müller-Krumbhaar and collaborators [9–11], where morphological structures and morphological transitions, from the type observed in this work, can be obtained. In single-component monolayers diffusion of heat is not the key factor, instead, the key factor is the area density difference between coexisting phases.

REFERENCES

[1]   Ben-Jacob E., *Contemp. Phys.*, **34** (1993) 247.
[2]   Langer J. S., *Rev. Mod. Phys.*, **52** (1980) 1.
[3]   Ben Amar M. and Pomeau Y., *Europhys. Lett.*, **2** (1986) 307.
[4]   Langer J. S., *Science*, **243** (1989) 1150.
[5]   Ihle I., *Eur. Phys. J. B*, **16** (2000) 337.
[6]   Utter B., Ragnarsson R. and Bodenschatz E., *Phys. Rev. Lett.*, **86** (2001) 4604.
[7]   Utter B. and Bodenschatz E., *Phys. Rev. E*, **72** (2005) 11601.
[8]   Brener E., Müller-Krumbhaar H. and Temkin D., *Europhys. Lett.*, **17** (1992) 535.
[9]   Brener E., Kassner K., Müller-Krumbhaar H. and Temkin D., *Int. J. Mod. Phys. C*, **3** (1992) 825.
[10] Brener E., Müller-Krumbhaar H. and Temkin D., *Phys. Rev. E*, **54** (1996) 2714.
[11] Brener E., Müller-Krumbhaar H., Temkin D. and Abel T., *Physica A*, **249** (1998) 73.
[12] Ihle T. and Müller-Krumbhaar H., *Phys. Rev. Lett.*, **70** (1993) 3083.
[13] Singer H. M. and Bilgram J. H., *Phys. Rev. E*, **70** (2001) 31601.
[14] Miller A. and Möhwald H. J., *Chem. Phys.*, **86** (1987) 4258.
[15] Akamatsu S., Bouloussa O., To K. and Rondelez F., *Phys. Rev. A*, **46** (1992) 4505.
[16] Weidemann G. and Vollhardt D., *Langmuir*, **13** (1997) 1623.
[17] Gehlert U. and Vollhardt D., *Langmuir*, **13** (1997) 277.
[18] Imura K., Yamauchi Y., Tsuchiya Y. Kato T. and Suzuki M., *Langmuir*, **17** (2001) 4602.
[19] Flores A., Ize P., Ramos S. and Castillo R., *J. Chem. Phys.*, **119** (2003) 5644.
[20] Bruinsma R., Rondelez F. and Levine A., *Eur. Phys. J. E*, **6** (2001) 191.
[21] Dougherty A., Kaplan P. D. and Gollub J. P., *Phys. Rev. Lett.*, **58** (1987) 1652.